

1 Third response to the comments of the Reviewer 1

2
3 **Atmospheric Band Fitting Coefficients Derived from Self-Consistent Rocket-Borne**
4 **Experiment.**

5 By M. Grygalashvily, M. Eberhart, J. Hedin, B. Strelnikov, F.-J. Lübken, M. Rapp, S. Löhle,
6 S. Fasoulas, M. Khaplanov, J. Gumbel, and E. Vorobeva

7
8 Dear Referee,

9
10 Thank you very much for your positive mark of our work and constructive corrections.
11 Almost all of your corrections were utilized.

12
13 Page 7. Line 155. Change "as a main one" to read "as the main one".

14 Changed.

15
16 Page 7. Line 161. I suggest to add and combine here lines 164-165 to read something similar
17 to: "Then the volume emission, V_{at} , is obtained multiplying the O_2b concentration by the
18 spontaneous emission coefficient of the (0-0) band, A_1 , of reaction R5 (hereafter,
19 nomenclature RX means the reaction X for table 1)".

20
21 We add such formulation at Line 161.

22
23 Page 10. Line 235. I suggest to change " 0.11 ± 0.018 " to read " 0.11 ± 0.02 ".

24 Changed.

25
26 Page. 14. Line 331. Add "the" to read: "is larger than the term with".

27 We add "the".

28
29 Page. 14. In my opinion the expression 5 can be introduced in line 353, by explaining that is
30 the expression derived from combined mechanism (expressions 1 and 3) that similar to two
31 step mechanism (is rearranged in expression 4) can be rearranged as: (Then, write expression
32 5). In my opinion I do not find necessary to repeat these expressions in an appendix.

33
34 We decided leave this place as it is. Please, approach with an understanding.

35
36
37
38
39
40
41
42
43
44
45
46
47
48
49
50
51
52
53
54
55
56
57
58
59
60
61
62
63
64
65
66
67
68

Page. 16. Line 380. Add ",alone," to read. "...direct excitation, alone, is less probable..."

Changed.

Page 16. Lines 395-396. Add the values "0.08" and "0.231" to read: "... of total efficiency $\alpha = 0.08$ and a ratio of $kO/KO_2 = 0.231$ for the two-step..."

It is corrected according with your suggestion.

Thank you a lot for taking your time to review our manuscript and for your comprehensive and unformal approach to our work.

With respect,

M. Grygalashvyly, M. Eberhart, J. Hedin, B. Strelnikov, F.-J. Lübken, M. Rapp, S. Löhle, S. Fasoulas, M. Khaplanov, J. Gumbel, and E. Vorobeva.

69 Second Response to the comments of the Reviewer 3

70

71 **Atmospheric Band Fitting Coefficients Derived from Self-Consistent Rocket-Borne**
72 **Experiment.**

73 By M. Grygalashvily, M. Eberhart, J. Hedin, B. Strelnikov, F.-J. Lübken, M. Rapp, S. Löhle,
74 S. Fasoulas, M. Khaplanov, J. Gumbel, and E. Vorobeva

75

76 Dear Referee,

77

78 Thank you very much for your positive mark of our work and constructive technical
79 corrections and suggestions. All of your corrections were utilized.

80

81 Line 538: write out acronyms (NLC, PMSE) once.

82 We add decipherment for NLC and PMSE.

83

84 Line 574: The essential step ... has been "made"

85 Changed.

86

87 Line 591: Capitals or not capitals? Use consistently

88 Changed.

89

90 Line 662-663: the sentence misses a verb, maybe "is in photochemical equilibrium"?

91 Corrected. We add "is".

92

93 Line 705-706: "is submitted true" should be "is assumed true"?

94 Yes, it should be "is assumed true". It is corrected.

95

96 Line 709: "such ability" better "such processes" or "the ability for such processes"?

97 We change this formulation. Now we write "such processes".

98

99 Line 750 and following: please just state what you used - error propagation from the
100 precursors, variance, fitting errors?

101 We add such statements.

102 Other changes are related to the corrections of other referee. Thank you a lot for taking your
103 time to review our manuscript and for your comprehensive and not formal approach to our
104 work.

105

106 With respect,

107 M. Grygalashvyly, M. Eberhart, J. Hedin, B. Strelnikov, F.-J. Lübken, M. Rapp, S. Löhle, S.
108 Fasoulas, M. Khaplanov, J. Gumbel, and E. Vorobeva.

109

110

111

112

113

114

115

116

117

118

119

120

121

122

123

124

125

126

127

128

129 **Atmospheric Band Fitting Coefficients Derived from Self-Consistent Rocket-Borne**

130 **Experiment**

131 Mykhaylo Grygalashvily¹, Martin Eberhart⁵, Jonas Hedin⁴, Boris Strelnikov¹, Franz-Josef
132 Lübken¹, Markus Rapp^{1,2}, Stefan Löhle⁵, Stefanos Fasoulas⁵, Mikhail Khaplanov^{4†}, Jörg
133 Gumbel⁴, and Ekaterina Vorobeva³

134 ¹Leibniz-Institute of Atmospheric Physics at the University Rostock in Kühlungsborn,
135 Schloss-Str. 6, D-18225 Ostseebad Kühlungsborn, Germany

136 ²Deutsches Zentrum für Luft- und Raumfahrt, Institut für Physik der Atmosphäre,
137 Oberpfaffenhofen, Germany

138 ³Department of Atmospheric Physics, Saint-Petersburg State University, Universitetskaya
139 Emb. 7/9, 199034, Saint-Petersburg, Russia

140 ⁴Department of Meteorology (MISU), Stockholm University, Stockholm, Sweden

141 ⁵University of Stuttgart, Institute of Space Systems, Stuttgart, Germany

142 [†]Deceased

143
144 **Abstract**

145 Based on self-consistent rocket-borne measurements of temperature, densities of atomic
146 oxygen and neutral air, and volume emission of the Atmospheric Band (762 nm) we
147 examined the one-step and two-step excitation mechanism of $O_2(b^1\Sigma_g^+)$ for night-time
148 conditions. Following McDade et al. (1986), we derived the empirical fitting coefficients,
149 which parameterize the Atmospheric Band emission $O_2(b^1\Sigma_g^+ - X^3\Sigma_g^-)(0,0)$. This allows to
150 derive atomic oxygen concentration from night-time observations of Atmospheric Band
151 emission $O_2(b^1\Sigma_g^+ - X^3\Sigma_g^-)(0,0)$. The derived empirical parameters can also be utilised for
152 Atmospheric Band modelling. Additionally, we derived fit function and corresponding
153 coefficients for combined (one- and two-step) mechanism. Simultaneous common volume

154 measurements of all the parameters involved in the theoretical calculation of the observed
155 $O_2(b^1\Sigma_g^+ - X^3\Sigma_g^-)(0,0)$ emission, i.e. temperature and density of the background air, atomic
156 oxygen density, and volume emission rate, is the novelty and the advantage of this work.

157

158 **1. Introduction**

159

160 The mesopause region is essential to understand the chemical and physical processes in the
161 upper atmosphere because this is region of coldest temperature (during summer at high
162 latitudes) and highest turbulence in the atmosphere (e.g. Lübken, 1997), the region of
163 formation of such phenomena as **noctilucent clouds** (NLC) and **polar mesospheric summer**
164 **echoes** (PMSE) (e.g. Rapp and Lübken, 2004), the region of gravity waves (GWs) breaking
165 and formation of secondary GWs (Becker and Vadas, 2018), as well as the region of coupling
166 between mesosphere and thermosphere. This region is characterised by different airglow
167 emissions and, particularly, by the emissions of the Atmospheric Band which is produced by
168 the excited state of molecular oxygen $O_2(b^1\Sigma_g^+)$. Airglow observation in the Atmospheric
169 Band is a useful method to study dynamical processes in the mesopause region. There have
170 been a number of reports of gravity waves (GWs) detection in this band (Noxon, 1978;
171 Viereck and Deehr, 1989; Zhang et al., 1993). Planetary wave climatology has been
172 investigated by the Spectral Airglow Temperature Imager (SATI) instrument (Lopez-
173 Gonzalez et al., 2009). In addition, the parameters of tides have been reported from SATI
174 (Lopez-Gonzalez et al., 2005) and High Resolution Doppler Imager (HRDI) observations
175 (Marsh et al., 1999). In number of works Sheese et al. (2010, 2011) inferred the temperature
176 by Atmospheric Band observation. Furthermore, the response of mesopause temperature and
177 atomic oxygen during major sudden stratospheric warming was studied utilising Atmospheric
178 Band emission by Shepherd et al. (2010). Various works have focused on Atmospheric Band
179 emission modelling with respect to gravity waves and tides (e.g. Hickey et al., 1993; Leko et

180 al., 2002; Liu and Swenson, 2003). The specific theory of the gravity wave effects on
181 $O_2(b^1\Sigma_g^+)$ emission was derived in Tarasick and Shepherd (1992). Moreover, Atmospheric
182 Band observations have been widely utilised to infer atomic oxygen, which is an essential
183 chemical constituent for energetic balance in the extended mesopause region (e.g. Hedin et
184 al., 2009, and references there in), and ozone concentration (Mlynczak et al., 2001). Although
185 there is a large field of application of Atmospheric Band emissions, there is a lack of
186 knowledge on processes of the $O_2(b^1\Sigma_g^+)$ population. Two main mechanisms of night-time
187 population (note, the day-time mechanisms are quite different, see e.g. Zarbo et al., (2018))
188 were proposed: the first is the direct population from three-body recombination of atomic
189 oxygen (e. g. Deans et al., 1976); the second is the so-called two-step mechanism, which
190 assumes an intermediate excited precursor O_2^* (e. g. Witt et al., 1984; Greer et al., 1981). It
191 has been shown by laboratory experiments that the first mechanism alone has not explained
192 observed emissions (Young and Sharpless, 1963; Clyne et al., 1965; Young and Black, 1966;
193 Bates, 1988). The second mechanism entails a discussion about the precursor excited state
194 and additional ambiguities in their parameters (e.g. Greer et al., 1981; Ogryzlo et al., 1984).
195 Thus, Witt et al. (1984) proposed the hypothesis that the $O_2(c^1\Sigma_u^-)$ state is, possibly, the
196 precursor; López-González et al. (1992a) suppose that the precursor could be $O_2(^5\Pi_g)$; Wildt
197 et al. (1991) found by laboratory measurements that it could be $O_2(A^3\Sigma_u^+)$. Hence, the
198 problem of identification is still not solved. The essential step in this direction has been ~~done~~
199 ~~made~~ after the ETON 2 (Energy Transfer in the Oxygen Nightglow) rocket experiment.
200 ETON 2 mission yielded empirical fitting parameters that allow either to quantify the
201 $O_2(b^1\Sigma_g^+)$ (and, consequently, volume emission) by known O, or atomic oxygen by known
202 volume emission values (McDade et al., 1986). Despite the significance of this work, the
203 temperature and density of air (necessary for derivation) were taken from CIRA-72 and
204 MSIS-83 (Hedin, 1983) models. This leads to some degree of uncertainty (e.g. Murtagh et al.,

205 1990). Thus, more solid knowledge on these fitting coefficients based on consistent
206 measurements of atomic oxygen, volume emission of Atmospheric Band, and temperature
207 and density of background atmosphere is desirable. In this paper we present common volume
208 measurements of these parameters performed in the course of WADIS-2 sounding rocket
209 mission. In the next section, we describe the rocket experiment and obtained data relevant for
210 our study. In section 3, to make the paper easier to understand, we repeat some theoretical
211 approximations from McDade et al. (1986). The obtained results of our calculations are
212 discussed in section 4. Concluding remarks and summary are given in the last section.

213

214 **2. Rocket experiment description**

215

216 The WADIS (Wave propagation and dissipation in the middle atmosphere: Energy budget and
217 distribution of trace constituents) sounding rocket mission aimed to simultaneously study the
218 propagation and dissipation of GWs and measure the concentration of atomic oxygen. It
219 comprised two field campaigns conducted at the Andøya Space Center (ASC) in northern
220 Norway (69°N, 16°E). The WADIS-2 sounding rocket was launched during the second
221 campaign on 5 March 2015 at 01:44:00 UTC, that is, night-time conditions. For a more
222 detailed mission description, the reader is referred to Strelnikov et al. (2017) and the
223 accompanying paper by Strelnikov et al. (2018).

224 The WADIS-2 sounding rocket was equipped with the CONE instrument to measure absolute
225 neutral air density and temperature with high spatial resolution, instrument for atomic oxygen
226 density measurements FIPEX (Flux Probe Experiment) and the Airglow Photometer for
227 atmospheric band (762 nm) volume emission observation.

228 CONE (COMbined measurement of Neutrals and Electrons), operated by IAP (Leibniz
229 Institute of Atmospheric Physics at the Rostock University), is a classical triode type
230 ionisation gauge optimised for a pressure range between 10^{-5} to 1 mbar. The triode system is

231 surrounded by two electrodes: Whilst the outermost grid is biased to +3 to +6 V to measure
232 electron densities at a high spatial resolution, the next inner grid (-15 V) is meant to shield the
233 ionisation gauge from ionospheric plasma. CONE is suitable for measuring absolute neutral
234 air number densities at altitude range between 70 and 120 km. To obtain absolute densities,
235 the gauges are calibrated in the laboratory using a high-quality pressure sensor, like a
236 Baratron. The measured density profile can be further converted to a temperature profile
237 assuming hydrostatic equilibrium. For a detailed description of the CONE instrument, see
238 Giebeler et al. (1993) and Strelnikov et al. (2013). Molecular oxygen and molecular nitrogen
239 are derived from CONE atmospheric number density measurements and partitioning
240 according to NRLMSISE-00 reference atmosphere (Picone et al., 2002).

241 The Airglow Photometer operated by MISU (Stockholm University, Department of
242 Meteorology) measures the emission of the molecular oxygen Atmospheric Band around 762
243 nm from the overhead column, from which volume emission rate is inferred by
244 differentiation. For airglow measurements in general, a filter photometer is positioned under
245 the nose cone viewing along the rocket axis with a defined field-of-view (FOV). For WADIS-
246 2 however, the FOV of $\pm 3^\circ$ was tilted from the rocket axis by 3° to avoid having other parts of
247 the payload within the FOV and at the same time roughly view the same volume as the other
248 instruments. The optical design is a standard radiometer-type system with an objective lens, a
249 field lens, aperture and stops which provide an even illumination over a large portion of the
250 detector surface (photomultiplier tube) and a defined FOV. At the entrance of the photometer
251 there is an interference filter with a passband of 6 nm centred at 762 nm. During ascent, after
252 the nosecone ejection, the photometer then counts the incoming photons from the overhead
253 column (or actually the overhead cone). When the rocket passes through the layer the
254 measured photon flux drops and above the emission layer only weak background emissions
255 are present (e.g. the zodiacal and galactic light). After the profile has been corrected for
256 background emissions and attitude (van Rhijn effect) it is converted from counts to radiance

257 using pre-flight laboratory calibrations. The calibration considers the spectral shape of the 0-0
258 band of the $O_2(b^1\Sigma_g^+ - X^3\Sigma_g^-)(0,0)$ Atmospheric Band system and the overlap of the
259 interference filter passband. The profile is then smoothed and numerically differentiated with
260 respect to altitude to yield the volume emission rate of the emitting layer. The data were
261 sampled with 1085 Hz which results in an altitude resolution of about 0.75 m during the
262 passage of the airglow layer (the velocity was ~ 800 m/s at 95 km). However, because of the
263 high noise level, the profile needed to be averaged to a vertical resolution of at least 3 km in
264 order to get satisfactory results after the differentiation. A more detailed description and
265 review of this measurement technique is given by Hedin et al. (2009).

266 The aim of the FIPEX developed by the IRS (Institute of Space Systems, University of
267 Stuttgart) is to measure the atomic oxygen density along the rocket trajectory with high spatial
268 resolution. It employs solid electrolyte sensor which has a selective sensitivity to atomic
269 oxygen. A low voltage is applied between anode and cathode pumping oxygen ions through
270 the electrolyte ceramic (yttria stabilised zirconia). The current measured is proportional to the
271 oxygen density. Sampling is realised with a frequency of 100 Hz and enables a spatial
272 resolution of ~ 10 m. Laboratory calibrations were done for molecular and atomic oxygen. For
273 a detailed description of the FIPEX instruments and their calibration techniques see Eberhart
274 et al. (2015, 2018).

275

276 **3. Theory**

277

278 Here, we are repeating the theory of $O_2(b^1\Sigma_g^+ - X^3\Sigma_g^-)(0,0)$ night-time emissions following
279 McDade et al. (1986) to make our paper more readable, using all nomenclature as in the
280 original paper. All utilised reactions are listed in Table 1, together with corresponding
281 reaction rates, branching ratios, quenching rates and spontaneous emission coefficients. Some

282 components have been updated according to modern knowledge, thus, deviating from the
 283 work of McDade et al. (1986).

284 Assuming direct one-step mechanism as **a the** main one for population and that the $O_2(b^1\Sigma_g^+)$
 285 **is** in photochemical equilibrium, we can write its concentration as a ratio of production to the
 286 loss term:

$$[O_2(b^1\Sigma_g^+)] = \frac{\varepsilon k_1 [O]^2 M}{A_2 + k_2^{O_2} [O_2] + k_2^{N_2} [N_2] + k_2^O [O]}, \quad (1)$$

287 where k_1 – reaction rate for three-body recombination of atomic oxygen, ε is the
 288 corresponding quantum yield of $O_2(b^1\Sigma_g^+)$ formation, A_2 represents the spontaneous emission
 289 coefficient, and $k_2^{O_2}, k_2^{N_2}, k_2^O$ are the quenching coefficients for reactions with O_2, N_2 and O ,
 290 respectively. **Then the volume emission, V_{at} , is obtained multiplying the $O_2(b^1\Sigma_g^+)$**
 291 **concentration by the spontaneous emission coefficient, A_1 , of reaction R5 (hereafter,**
 292 **nomenclature RX means the reaction X for Table 1).**

293 In case of known temperature, volume emission and concentrations of O, O_2, N_2 , and M , the
 294 quantum yield of $O_2(b^1\Sigma_g^+)$ formation can be calculated as follows:

$$\varepsilon = V_{at} \frac{A_2 + k_2^{O_2} [O_2] + k_2^{N_2} [N_2] + k_2^O [O]}{A_1 k_1 [O]^2 M}. \quad (2)$$

295 ~~where A_1 is spontaneous emission for reaction R5 (hereafter, nomenclature RX means the~~
 296 ~~reaction X from Table 1).~~

297 In the case of the two-step mechanism, the unknown excited state O_2^* is populated at the first
 298 step from the reaction R7. Then, it can be deactivated by quenching (R9), spontaneous
 299 emission (R10) or producing $O_2(b^1\Sigma_g^+)$ by the reaction R8. Note, R8 is one pathway of the
 300 overall quenching reaction R9.

301 In the second step, O_2^* is transformed into $O_2(b^1\Sigma_g^+)$, which, can be deactivated by quenching
 302 (R2-R4) and by spontaneous emission (R6). Assuming photochemical equilibrium for O_2^* and,
 303 as before, for $O_2(b^1\Sigma_g^+)$ the volume emission in the case of $O_2(b^1\Sigma_g^+ - X^3\Sigma_g^-)(0,0)$ is:

$$V_{at} = \frac{A_1 \alpha k_1 [O]^2 M \gamma k_3^{O_2} [O_2]}{(A_2 + k_2^{O_2} [O_2] + k_2^{N_2} [N_2] + k_2^O [O]) (A_3 + k_3^{O_2} [O_2] + k_3^{N_2} [N_2] + k_3^O [O])}, \quad (3)$$

304 where quantum yield of O_2^* formation α , quantum yield of $O_2(b^1\Sigma_g^+)$ formation γ ,
 305 spontaneous emission coefficient A_3 , and $k_3^{O_2}, k_3^{N_2}, k_3^O$ unknown quenching rates of O_2^* . Note,
 306 assumption about photochemical equilibrium for O_2^* and $O_2(b^1\Sigma_g^+)$ is valid, because
 307 $O_2(b^1\Sigma_g^+)$ radiative lifetime is less than 12 s and all potential candidates for of O_2^* have
 308 lifetime less than several seconds (e.g. López-González et al., 1992a, 1992b, 1992c;
 309 Yankovsky et al., 2016, and references therein).

310 Collecting all known values on the right-hand side (RHS) and all unknown summands on the
 311 left-hand side (LHS), omitting emissive summand A_3 as non-effective loss (McDade et al.,
 312 1986) equation (3) can be rearranged as follows:

$$C^{O_2} [O_2] + C^O [O] = \frac{A_1 k_1 [O]^2 M [O_2]}{V_{at} (A_2 + k_2^{O_2} [O_2] + k_2^{N_2} [N_2] + k_2^O [O])}, \quad (4)$$

313 where $C^{O_2} = (1 + k_3^{N_2} [N_2] / k_3^{O_2} [O_2]) / \alpha \gamma$ and $C^O = k_3^O / \alpha \gamma k_3^{O_2}$ are the fitting coefficients
 314 that can be calculated by the least square fit (LSF) procedure. Such derivation assumes that
 315 the coefficients are temperature independent (or temperature dependence is weak). This
 316 means that the reaction rates k_3 are assumed to be temperature independent (dependence is
 317 weak), or have the same temperature dependency for all quenching partners (N_2, O_2, O).
 318 Currently, this statement on the basis of available information about potential precursors is
 319 **submitted assumed** true, but for which the solid evidence is absent. We calculated them based
 320 on our measurements and will discuss the results in the following section.

321 In more general case population of $O_2(b^1\Sigma_g^+)$ occurs via both channels: one-step and two-
322 step. We discuss such **ability processes** in section 4.3 and derive an expression for
323 corresponding fit-function in Appendix.

324

325 **4. Results and discussion**

326

327 Figure 1 shows input data for our calculations: temperature from CONE instrument (Fig. 1a),
328 number density of air (Fig. 1b), atomic oxygen concentration measured by FIPEX (Fig. 1c)
329 and volume emission at 762 nm from photometric instrument (Fig. 1d). A temperature
330 minimum of ~158 K was observed at 104.2 km. A local temperature peak was measured at
331 98.9 km with values of 204.5 K. The secondary temperature minimum was visible at 95.4 km
332 and amounted to ~173 K. Atomic oxygen concentration (Fig. 1c) had a peak of $\sim 4.7 \cdot 10^{11}$ [cm⁻³]
333] at 97.2 km and approximately coincided with the secondary temperature peak. The peak of
334 volume emission was detected between 95 and 97 km with values of more than 1700
335 [phot·cm⁻³·s⁻¹]; this is slightly beneath the atomic oxygen corresponding maximum and
336 slightly above the secondary temperature minimum. Note, this point to the competition of the
337 temperature and the atomic oxygen concentration in the processes of atomic oxygen excited
338 state $O_2(b^1\Sigma_g^+)$ formation. Independently of the mechanism of atmospheric band emission
339 (Eq. 1 or Eq. 3), the numerator is directly proportional to the square of atomic oxygen
340 concentration and inversely proportional to the third power of the temperature (via reaction
341 rate k_I and M , considering the ideal gas law). Our rocket experiment shows an essential
342 difference of emissions between ascending and descending flights (see Strelnikov et al.,
343 2018). It also demonstrates a significant variability in other measured parameters, including
344 neutral temperature and density as well as atomic oxygen density (Strelnikov et al., 2017,
345 2018). This suggests that, in the case of the ETON 2 experiments, the temporal extrapolation
346 of atomic oxygen for the time of the emission measurement flight (which was approximately

347 20 min earlier) may lead to serious biases in estimations because, as one can see from Eq. 1
348 and Eq. 3, volume emission depends on the atomic oxygen concentration quadratically. Since
349 the best quality data were obtained during the descent of the WADIS-2 rocket flight, we chose
350 this data set for our analysis (Strelnikov et al., 2018). The region above 104 km is subject to
351 auroral contamination. In the region below 92 km, negative values may occur in the volume
352 emission profile as the result of self-absorption in the denser atmosphere below the emission
353 layer. Hence, we considered the region near the peak of emission between 92 km and 104 km
354 as most appropriate for our study. The comparisons of our measurements with other
355 observations, as well as with the results of modelling are presented in several papers (e.g.
356 Eberhart et al., 2018; Strelnikov et al., 2018).

357

358 **4.1 One-step mechanism**

359

360 Figure 2 shows the quantum yield of $O_2(b^1\Sigma_g^+)$ formation ε calculated according to Eq. (2),
361 which is necessary to form $O_2(b^1\Sigma_g^+)$ under the assumption that the direct three-body
362 recombination of atomic oxygen is the main mechanism. The uncertainties for this figure (as
363 well as for other figures) were calculated according with sensitivity analysis (von Clarmann,
364 2014; Yankovsky and Manuilova, 2018, (Appendix 1); Vorobeva et al., 2018), **where the**
365 **errors represent error propagation from the experimental data.** Calculated values of ε are
366 placed in the range [0.07; 0.13], which is in good agreement with the values derived by
367 McDade et al. (1986). The averaged value amounts to 0.11 ± 0.02 . The range of values taking
368 into account both the variance and the error range amounts to [0.02; 0.22]. By the physical
369 nature of this value, the quantum yield of $O_2(b^1\Sigma_g^+)$ formation should not depend on altitude.
370 Fig. 2 shows some altitude dependence of central values of ε , but considering the large error
371 range, there is no clear altitude dependence. The variability of the data points is much smaller

372 than the errors of the individual points. Hence, in light of the analysis of our rocket
373 experiment, we may not decline direct excitation mechanism.

374 Although the population via one-step mechanism alone is, generally speaking, possible, it is
375 improbable because laboratory experiments show that the direct excitation alone may not
376 explain observed emissions (Young and Sharpless, 1963; Clyne et al., 1965; Young and
377 Black, 1966; Bates, 1988). This conclusion is in agreement with the conclusion from McDade
378 et al. (1986), which stated that the one-step excitation mechanism is not sufficient to explain
379 the $O_2(b^1\Sigma_g^+)$ population. Hence, in the following, we check the second energy transfer
380 mechanism.

381

382 **4.2 Two-step mechanism**

383

384 Figure 3 depicts the altitude profile of the right hand side (RHS) of equation (4) and profile
385 calculated by the least-square fit (LSF). The fitting coefficients, C^{O_2} and C^O , resulting from
386 this fit, amount to $9.8_{+6.5}^{-5.3}$ and $2.1_{-0.6}^{+0.3}$, respectively. The uncertainties were calculated, as
387 commonly for LSF (Bevington and Robinson, 2003), **based on error propagation from the**
388 **RHS as provided in Figure 3.** Our C^{O_2} coefficient is partially, within the error range, in
389 agreement with C^{O_2} coefficients given in McDade et al. (1986), which amount to 4.8 ± 0.3 and
390 6.6 ± 0.4 for temperature from CIRA-72 and MSIS-83, respectively. The C^O coefficient is
391 approximately one order lower. There are several possible reasons for the large discrepancy in
392 C^O , for example the temperature dependence of the O-quenching or that, in the case of ETON
393 2 experiments mean temperature profiles from the models CIRA-72 and MSIS-83 were
394 utilized, which does not reproduce any short-time dynamical fluctuations, solar cycle
395 conditions, etc. In frame of our analysis, we may not identify the reason for the large
396 discrepancy in C^O more precisely. Fitting coefficients defined in such a way (Eq. 4) do not
397 have a direct physical meaning. However, they have a physical meaning in several limit cases.

398 If the quenching coefficients of a precursor with molecular nitrogen are much smaller than
 399 those with molecular oxygen ($k_3^{N_2} \ll k_3^{O_2}$), then $\alpha\gamma = 1/C^{O_2}$. The assumption, that the
 400 quenching of the precursor with N_2 is much slower than quenching with O_2 , is just working
 401 hypothesis, which is commonly used for analysis of possible precursor (e.g. McDade et al.,
 402 1986; López-González et al, 1992a, 1992b; and references therein). It is true for such potential
 403 precursor as $O_2(A^3\Sigma_u^+)$ (Kenner and Ogryzlo, 1983b), but generally, there is no evidence,
 404 neither for nor against that. If it is not true, any definite conclusion on precursor by known
 405 C^{O_2} is not possible. In our case $\alpha\gamma = 0.102_{-0.041}^{+0.120}$. In other words, in the case of two-step
 406 formation of $O_2(b^1\Sigma_g^+)$ with energy transfer agent O_2 , the total efficiency $\eta = \alpha\gamma$ amounts to
 407 10.2%, which is the lowest amongst known values. Based on rocket experiment data analysis
 408 (ETON), Witt et al. (1984) obtained $\alpha\gamma = 0.12 - 0.2$. According to McDade et al. (1986), for
 409 the case with $k_2^O = 8 \cdot 10^{-14}$, the total efficiencies are 0.15 and 0.21 for temperature profiles
 410 adopted from MSIS-83 and CIRA-72, respectively. The analyses of López-González et al.
 411 (1992a, c), adopted O_2 , N_2 , and temperature profiles from the model (Rodrigo et al., 1991),
 412 showed a total efficiency of 0.16. In contrast to our work, all investigations mentioned above
 413 utilised the temperature and atmospheric density from models which describe a mean state of
 414 the atmosphere. This is a possible reason for discrepancy in the results. Total efficiency η may
 415 serve as an auxiliary quantity to identify the precursor. According to the physical meaning of
 416 efficiency, it may not be larger than 1. Hence, α , γ , as well as the total efficiency are smaller
 417 than 1. Consequently, $\gamma = \eta/\alpha < 1$, and we can examine potential candidates for O_2^* with this
 418 criterion. From an energetic point of view, only four bound states of molecular oxygen can be
 419 considered as an intermediate state for the $O_2(b^1\Sigma_g^+)$ population:
 420 $O_2(A^3\Sigma_u^+)$, $O_2(A'^3\Delta_u)$, $O_2(c^1\Sigma_u^-)$, and $O_2(^5\Pi_g)$ (Greer et al., 1981; Wraight, 1982; Witt et al.,
 421 1984; McDade et al., 1986; López-González et al., 1992c). For better readability, we will
 422 partially repeat a table from López-González et al. (1992b, c) with known α in our work

423 (Table 2). From Table 2, it can be seen that only $O_2(A'^3\Delta_u)$ and $O_2(^5\Pi_g)$ fit to the criterion of
 424 $\gamma = 0.102/\alpha < 1$. At lower limit of uncertainty ($\gamma = 0.061/\alpha < 1$) $O_2(A'^3\Delta_u)$ and $O_2(^5\Pi_g)$
 425 satisfy to the criterion, and considering upper limit ($\gamma = 0.222/\alpha < 1$), only $O_2(^5\Pi_g)$ may
 426 serve as precursor.

427 The second expression that helps to clarify the choice of the precursor is the ratio of
 428 quenching rates. In the limit of low quenching with molecular nitrogen ($k_3^{N_2} \ll k_3^{O_2}$), the ratio
 429 of fitting coefficients equals the ratio of the quenching rates of atomic and molecular oxygens
 430 ($C^0/C^{O_2} = k_3^O/k_3^{O_2}$). An analysis from the ETON 2 rocket experiment yields values of
 431 quenching coefficients ratios of potential precursor of 3.1 and 2.9 for temperatures from
 432 CIRA-72 and MSIS-83, respectively. This is close to the value from Ogryzlo et al. (1984),
 433 who found $k_3^O/k_3^{O_2} = 2.6$ by laboratory measurements; however, as was noted in their work,
 434 substitution of these values into the equation for emission yields 16 % of the observed
 435 emission (Ogryzlo et al., 1984). These findings point to the possibility of a too high measured
 436 ratio $k_3^O/k_3^{O_2}$ as the result of too strong quenching of precursor by atomic oxygen. Our value
 437 of quenching ratios $k_3^O/k_3^{O_2}$ amounts to $0.21_{-0.12}^{+0.32}$. There is not enough information on
 438 measured values for bound states of molecular oxygen. Laboratory measurements for
 439 $O_2(A^3\Sigma_u^+)(v = 0 - 4)$, $O_2(A^3\Sigma_u^+)(v = 2)$, and $O_2(c^1\Sigma_u^-)$ infer the values of $k_3^O/k_3^{O_2}$ ratio to
 440 be 30 ± 30 , 100 ± 15 , and 200 ± 20 , respectively (Kenner and Ogryzlo, 1980; Kenner and
 441 Ogryzlo, 1983a, 1983b; Kenner and Ogryzlo, 1984). On the other hand, Slanger et al. (1984)
 442 found a lower limit of $O_2(A^3\Sigma_u^+)(v = 8)$ quenching by O_2 must be $\geq 8 \cdot 10^{-11}$. If the results
 443 from Slanger et al. (1984) were applied to the results from Kenner and Ogryzlo (1980, 1984)
 444 for $k_3^{O_2}$, then the ratio of $k_3^O/k_3^{O_2}$ would be two orders lower. This short discussion illustrates a
 445 strong scattering of this ratio. For our two potential candidates ($O_2(A'^3\Delta_u)$ and $O_2(^5\Pi_g)$),
 446 there is information about $k_3^O/k_3^{O_2}$ ratio for only $O_2(A'^3\Delta_u)$. Through the comprehensive

447 analysis of known rocket experiments, López-González et al. (1992a, b, c) inferred that the
448 upper limit of the ratio amounts to 1. Hence, our value of $k_3^O/k_3^{O_2} = 0.21_{-0.12}^{+0.32}$ agrees with
449 this result. Consistent information from laboratory experiments on the ratio for $O_2(^5\Pi_g)$ is
450 absent. Thus, we can propose as potential candidates for precursor both $O_2(A^3\Delta_u)$ and
451 $O_2(^5\Pi_g)$; however, we are not able to identify which of these two is more preferable.

452 In order to illustrate the application of the newly derived fitting coefficients we compare in
453 Figure 4 the atomic oxygen concentration from FIPEX (black line), from NRL MSISE-00
454 reference atmosphere model (Picone et al., 2002) (red line); calculated with McDade et al.
455 (1986) coefficients (blue line), and with our fitting coefficients for the two-step mechanism
456 (green line). In the region 94-98 km, i.e. at atomic oxygen peak and volume emission peak
457 (see Fig. 1d) fitting coefficients from this paper better than McDade coefficients (MSIS-83
458 case) reproduce observed values. Our fitting coefficients and fitting coefficients of McDade
459 give similar approximation above atomic oxygen peak (~98-104 km). The shape of the
460 calculated profiles appears slightly different, with the peak maximum at a higher altitude than
461 the observed. In this, our result resembles the McDade results, probably because in both
462 cases, the ratio of two reaction rates is derived, but not the rates themselves. In the lower part
463 our results and those of McDade differ, because our C^{O_2} value is larger and the term with
464 molecular oxygen dominates. Nevertheless, the atomic oxygen retrieved with our fitting
465 coefficients satisfactorily reproduces measurements, especially at the peak.

466

467 **4.3 Combined mechanism**

468

469 In the most general case, the $O_2(b^1\Sigma_g^+)$ population passes through two channels: directly and
470 via precursor. In fact, theoretical calculations from Wraight (1982) and laboratory
471 measurements from Bates (1988) predicted a direct population with efficiencies of 0.015 and

472 0.03, respectively, which is not sufficient to explain the observed emissions (Bates, 1988,
 473 Greer et al., 1981; Krasnopolsky, 1986). A similar value, $\varepsilon=0.02$, was shown in the analysis
 474 by López-González et al. (1992b, c). We investigated a combined mechanism based on the
 475 LSF calculation and fit function (derivation in Appendix):

$$\frac{[O_2] + D_1[O]}{D_2 + \tilde{\varepsilon}(1 + D_1[O]/[O_2])} = \frac{A_1 k_1 [O]^2 M [O_2]}{V_{at}(A_2 + k_2^{O_2} [O_2] + k_2^{N_2} [N_2] + k_2^O [O])}, \quad (5)$$

476 where, hereafter, tildes denote that these are values for combined mechanism and do not equal
 477 to the values for one-step or two-step mechanisms (Sec. 4.1 and 4.2); $D_1 = \tilde{k}_3^O / \tilde{k}_3^{O_2}$ and
 478 $D_2 = \tilde{\alpha}\tilde{\gamma}$ are the fitting coefficients, which refer to the ratio of quenching rates and $\tilde{\eta} \equiv \tilde{\alpha}\tilde{\gamma}$
 479 total efficiency for two-step channel, respectively. The fitting coefficients were calculated for
 480 two limit cases $\tilde{\varepsilon}=0.015$ (Wraight, 1982), $\tilde{\varepsilon}=0.03$ (Bates, 1988) and for the averaged case
 481 $\tilde{\varepsilon}=0.022$.

482 The results for the best-fit in each case are listed in Table 3. Analogously to the two-step
 483 mechanism (Sec. 4.2), for the case of combined mechanism $\tilde{\gamma} = \tilde{\eta}/\tilde{\alpha} < 1$, hence, the
 484 precursor should satisfy $\tilde{\alpha} > 0.08_{-0.04}^{+0.12}$ (see Tab. 3). For central values of $\tilde{\alpha}$, only $O_2(A'^3\Delta_u)$
 485 and $O_2(^5\Pi_g)$ satisfy this criterion (see Tab. 2). At lower limit of uncertainty ($\tilde{\alpha} >$
 486 0.04) $O_2(A'^3\Delta_u)$, $O_2(A^3\Sigma_u^+)$, and $O_2(^5\Pi_g)$ satisfy to the criterion, and considering upper limit
 487 ($\tilde{\alpha} > 0.2$), only $O_2(^5\Pi_g)$ may serve as precursor. The upper limit of the ratio $k_3^O/k_3^{O_2} < 1$ for
 488 $O_2(A'^3\Delta_u)$, derived by López-González et al. (1992a, b, c), is in agreement with our
 489 calculations ($0.231_{-0.142}^{+0.358}$). As it is noted above, the ratio for $O_2(^5\Pi_g)$ is unknown.
 490 Consequently, taking into an account both conditions, only $O_2(A'^3\Delta_u)$ and $O_2(^5\Pi_g)$ may
 491 serve as precursor.

492 Figure 5 illustrates a sanity check for volume emissions derived (black lines) with fitting
 493 coefficients of McDade et al. (1986) for MSIS-83 (Fig. 5c) case and CIRA-72 case (Fig. 5d),
 494 and with our newly derived fitting coefficients for two-step (Fig. 5a) and combined ($\tilde{\varepsilon} =$

495 0.022) mechanisms (Fig. 5b) in comparison with measured one (red lines). All of derived
496 volume emission profiles (black lines) were calculated based on the temperature,
497 concentration of surrounding air, and concentration of atomic oxygen from our rocket launch.
498 The calculations with combined mechanism (Eq. 5) and two-step energy transfer mechanism
499 (Eq. 4) give almost identical results. The results obtained with new fitting coefficients are in
500 satisfactory agreement with the measured volume emissions at the peak and above, whereas
501 the McDade coefficients related to the temperature from CIRA-72 give better approximations
502 below the volume emission peak (92 km). The coefficients of McDade related to the
503 temperature from MSIS-83 are in better agreement with our results and are almost identical
504 above the volume emission peak. More independent common volume in-situ measurements
505 are necessary to validate these results.

506

507 **5. Summary and conclusions**

508

509 Based on the rocket-born common volume simultaneous observations of atomic oxygen,
510 atmospheric band emission (762 nm), and density and temperature of the background
511 atmosphere, the mechanisms of $O_2(b^1\Sigma_g^+)$ formation were analysed. Our calculations show
512 that one-step direct excitation **alone** is less probable by the reasons discussed above (Sec. 4.1).
513 For the case of the two-step mechanism, we found new coefficients for fit function in
514 accordance with McDade et al. (1986), based on self-consistent temperature, atomic oxygen
515 and volume emission observation. These coefficients amounted to $C^{O_2}=9.8_{+6.5}^{-5.3}$ and
516 $C^O=2.1_{-0.6}^{+0.3}$. C^{O_2} coefficient is partially, within the error range, in agreement with C^{O_2}
517 coefficients given in McDade et al. (1986), and C^O coefficient is approximately one order
518 lower. The general implication of these results is parameterisation of volume emission in
519 terms of known atomic oxygen. This can be utilised either for atmospheric band volume
520 emission modelling or for estimation of atomic oxygen by known volume emission. We

521 identified two candidates for the intermediate state of O_2^* . Our results show that $O_2(A'^3\Delta_u)$ or
 522 $O_2(^5\Pi_g)$ may serve as a precursor.

523 Taking into account both channels of $O_2(b^1\Sigma_g^+)$ formation, we proposed a combined
 524 mechanism. In this case, atomic oxygen via volume emission or volume emission based on
 525 known atomic oxygen can be calculated by equation (5). Recommended fitting coefficients
 526 amounted to $D_1=0.231_{-0.142}^{+0.358}$ and $D_2=0.08_{-0.04}^{+0.12}$, with the efficiency of the direct channel as
 527 $\tilde{\epsilon} = 0.022$. These coefficients have a meaning of total efficiency ($\tilde{\alpha}\tilde{\gamma} = 0.08_{-0.04}^{+0.12}$) and a ratio
 528 of quenching coefficients ($\tilde{k}_3^O/\tilde{k}_3^{O_2} = 0.231_{-0.142}^{+0.358}$) for the two-step channel. The analysis of
 529 their values indicates that $O_2(A'^3\Delta_u)$ and $O_2(^5\Pi_g)$ may serve as possible precursors for the
 530 two-step channel at combined mechanism. In the context of our rocket experiment, we do not
 531 have the possibility to figure out which mechanism is true. Nevertheless, we consider the
 532 combined mechanism as more relevant to nature, because it has a higher generality. This
 533 conclusion does not contradict to the current point of view that the two-step mechanism is
 534 dominant because $\tilde{\epsilon}$ is assumed to be 1.5-3 %. Moreover, it is possible that in the reality the
 535 mechanism is much more complex and it has multi-channel or more than two-step nature.
 536 Undoubtedly, more common volume simultaneous observations of the Atmospheric Band and
 537 the atomic oxygen concentrations would be desirable to confirm and improve these results.

538

539 **Appendix.**

540

541 We consider photochemical equilibrium for the night-time $O_2(b^1\Sigma_g^+)$ concentration. If
 542 $O_2(b^1\Sigma_g^+)$ is produced via both channels, the equilibrium concentration is given by the
 543 following expression:

$$[O_2(b^1\Sigma_g^+)] = \frac{\tilde{\epsilon}k_1[O]^2M + \tilde{\gamma}\tilde{k}_3^{O_2}[O_2][O_2^*]}{A_2 + k_2^{O_2}[O_2] + k_2^{N_2}[N_2] + k_2^O[O]}, \quad (A1)$$

544 where the tilde denotes the combined mechanism, $A_1, k_1, k_2^{O_2}, k_2^{N_2}, k_2^O, \tilde{k}_3^{O_2}$ are the ratios for
 545 corresponding processes (see Tab. 1) and O_2^* is the unknown precursor.

546 Considering this precursor in photochemical equilibrium, we can obtain the following
 547 expression for its concentration:

$$[O_2^*] = \frac{\tilde{\alpha} k_1 [O]^2 M}{\tilde{A}_3 + \tilde{k}_3^{O_2} [O_2] + \tilde{k}_3^{N_2} [N_2] + \tilde{k}_3^O [O]}, \quad (A2)$$

548 where efficiency $\tilde{\alpha}$, \tilde{A}_3 is the unknown spontaneous emission coefficient of O_2^* and
 549 $\tilde{k}_3^{O_2}, \tilde{k}_3^{N_2}, \tilde{k}_3^O$ are the unknown quenching rates for O_2^* .

550 Substituting A2 into A1 and into expression for volume emission we obtain:

$$\begin{aligned} 551 \quad V_{at} &= A_1 [O_2 (b^1 \Sigma_g^+)] = \\ &= \frac{A_1 k_1 [O]^2 [O_2] M}{A_2 + k_2^{O_2} [O_2] + k_2^{N_2} [N_2] + k_2^O [O]} \left(\frac{\tilde{\varepsilon}}{[O_2]} + \frac{\tilde{\alpha} \tilde{\gamma} \tilde{k}_3^{O_2}}{\tilde{A}_3 + \tilde{k}_3^{O_2} [O_2] + \tilde{k}_3^{N_2} [N_2] + \tilde{k}_3^O [O]} \right). \end{aligned} \quad (A3)$$

552 We assume that, in analogy with two-step mechanism, a spontaneous emission \tilde{A}_3 of O_2^* is
 553 much smaller than the quenching, and we utilised traditional assumption about low quenching
 554 with molecular nitrogen ($\tilde{k}_3^{N_2} \ll \tilde{k}_3^{O_2}$), which is commonly used to analyse a potential
 555 precursor. In this case, A3 can be rearranged as follows:

$$\frac{[O_2] + \frac{\tilde{k}_3^O}{\tilde{k}_3^{O_2}} [O]}{\tilde{\alpha} \tilde{\gamma} + \tilde{\varepsilon} \left(1 + \frac{\tilde{k}_3^O}{\tilde{k}_3^{O_2}} [O] / [O_2] \right)} = \frac{A_1 k_1 [O]^2 M [O_2]}{V_{at} (A_2 + k_2^{O_2} [O_2] + k_2^{N_2} [N_2] + k_2^O [O])}. \quad (A4)$$

556 We defined unknown fitting coefficients $D_1 \equiv \tilde{k}_3^O / \tilde{k}_3^{O_2}$ and $D_2 \equiv \tilde{\alpha} \tilde{\gamma}$. Expression A4 was
 557 utilised to calculate them with LSF.

558

559 **Acknowledgements.**

560

561 The authors are thankful to Prof. Dr. V. A. Yankovsky, Prof. Dr. W. Ward, and PD Dr. G. R.
562 Sonnemann for helpful suggestions and useful discussions. This work was supported by the
563 German Space Agency (DLR) under grant 50 OE 1001 (project WADIS). The authors thank
564 DLR-MORABA for their excellent contribution to the project by developing the complicated
565 WADIS payload and campaign support together with the Andøya Space Center, as well as H.-
566 J. Heckl and T. Köpnick for building the rocket instrumentation. The authors are thankful to
567 co-editor Dr. Bernd Funke for help in evaluating this paper and to three anonymous referees
568 for their useful comments and improvements of the paper.

569 The rocket-borne measurements and calculated data shown in this paper are available via
570 IAP's ftp server at <ftp://ftp.iap-kborn.de/data-in-publications/GrygalashvylyACP2018>.

571

572 **References**

573

574 Bates, D. R.: Excitation and quenching of the oxygen bands in the nightglow, *Planet. Space*
575 *Sci.*, **36(9)**, 875-881, 1988.

576

577 Becker, E., and Vadas, S. L.: Secondary gravity waves in the winter mesosphere: Results
578 from a high-resolution global circulation model, *J. Geophys. Res.*, **123**, 2605-2627,
579 doi:10.1002/2017JD027460, 2018.

580

581 Bevington, P. R., and Robinson, D. K.: Data reduction and error analysis for the physical
582 sciences, 3rd edition, published by McGraw-Hill Companies Inc., ISBN 0-07-247227-8,
583 2003.

584

585 Campbell, I. M. and Gray, C. N.: Rate constants for O(³P) recombination and association with
586 N(4S), *Chem. Phys. Lett.*, **8**, 259, 1973.

587

588 von Clarmann, T.: Smoothing error pitfalls, *Atmos. Meas. Tech.*, **7**, 3023-3034,
589 <https://doi.org/10.5194/amt-7-3023-2014>, 2014.

590

591 Clyne, M. A. A., Thrush, B. A., and Wayne, R. P.: The formation and reactions of metastable
592 oxygen ($b^1\Sigma_g^+$) molecules, *J. Photochem. Photobiol.*, **4**, 957, 1965.

593

594 Deans, A. J., Shepherd, G. G., and Evans, W. F. J.: A rocket measurement of the $O_2(b^1\Sigma_g^+ -$
595 $X^3\Sigma_g^-)$ atmospheric band nightglow altitude distribution, *Geophys. Res. Lett.*, **3(8)**, 441-444,
596 1976.

597

598 Eberhart, M., Löhle, S., Steinbeck, A., Binder, T., and Fasoulas, S.: Measurement of atomic
599 oxygen in the middle atmosphere using solid electrolyte sensors and catalytic probes,
600 *Atmospheric Measurement Techniques*, **8**, 3701–3714, doi:10.5194/amt-8-3701-2015, 2015.

601

602 Eberhart, M., Löhle, S., Strelnikov, B., Fasoulas, S. and Lübken, F.-J. Hedin, J., Khaplanov,
603 M., Gumbel, J.: Atomic oxygen number densities in the MLT region measured by solid
604 electrolyte sensors on WADIS-2, *Atmospheric Measurement Techniques*, submitted, 2018.

605

606 Giebeler, J., Lübken, F.-J., and Nägele, M.: CONE – a new sensor for in-situ observations of
607 neutral and plasma density fluctuations, ESA SP, Montreux, Switzerland, ESA-SP-355, 311–
608 318, 1993.

609

610 Greer, R. G. H., Llewellyn, E. J., Solheim, B. H., and Witt, G.: The excitation of $O_2(b^1\Sigma_g^+)$ in
611 the nightglow, *Planet. Space Sci.*, **29**, 383, 1981.

612
613
614
615
616
617
618
619
620
621
622
623
624
625
626
627
628
629
630
631
632
633
634
635
636
637

Hedin, A. E.: A revised thermospheric model based on mass spectrometer and incoherent scatter data: MSIS-83, *J. Geophys. Res.*, **88**, 10.170, 1983.

Hedin, J., Gumbel, J., Stegman, J., and Witt, G.: Use of O₂ airglow for calibrating direct atomic oxygen measurements from sounding rockets, *Atmos. Meas. Tech.*, **2**, 801–812, 2009.

Hickey, M. P., Schubert, G., and Walterscheid, R. L.: Gravity wave-driven fluctuations in the O₂ atmospheric (0–1) nightglow from an extended, dissipative emission region, *J. Geophys. Res.*, **98**, 717–730, 1993.

Kenner, R. D. and Ogryzlo, E. A.: Deactivation of O₂(A³Σ_u⁺) by O₂, O and Ar, *Int. J. Chem. Kinetics*, **12**, 501, 1980.

Kenner, R. D. and Ogryzlo, E. A.: Quenching of O₂(c¹Σ_u⁻, v = 0) by O(³P), O₂(a¹Δ_g) and other gases, *Can. J. Chem.*, **61**, 921, 1983a.

Kenner, R. D. and Ogryzlo, E. A.: Rate constant for the deactivation of O₂(A³Σ_u⁺) by N₂, *Chem. Phys. Lett.*, **103**, 209, 1983b.

Kenner, R. D. and Ogryzlo, E. A.: Quenching of O₂(A_{v=2} – X_{v=5}) Herzberg I band by O₂(a) and O, *Can. J. Phys.*, **62**, 1599, 1984.

Krasnopolsky, V. A.: Oxygen emissions in the night airglow of the Earth, Venus and Mars, *Planet. Space Sci.*, **34**, 511, 1986.

638 Leko, J. J., M. P. Hickey, and Richards, P. G.: Comparison of simulated gravity wave-driven
639 mesospheric airglow fluctuations observed from the ground and space, *J. Atmos. Solar-Terr.*
640 *Phys.*, **64**, 397– 403, 2002.

641

642 Liu, A. Z. and Swenson, G. R.: A modeling study of O₂ and OH airglow perturbations
643 induced by atmospheric gravity waves, *J. Geophys. Res.*, **108(D4)**, 4151,
644 doi:10.1029/2002JD002474, 2003.

645

646 López-González, M. J., López-Moreno, J. J., and Rodrigo, R.: Altitude profiles of the
647 atmospheric system of O₂ and of the green line emission, *Planet. Space Sci.*, **40(6)**, 783-795,
648 1992a.

649

650 López-González, M. J., López-Moreno, J. J., and Rodrigo, R.: Altitude and vibrational
651 distribution of the O₂ ultraviolet nightglow emissions, *Planet. Space Sci.*, **40(7)**, 913-928,
652 1992b.

653

654 López-González, M. J., López-Moreno, J. J., and Rodrigo, R.: Atomic oxygen concentrations
655 from airglow measurements of atomic and molecular oxygen emissions in the nightglow,
656 *Planet. Space Sci.*, **40(7)**, 929-940, 1992c.

657

658 Lopez-Gonzalez, M. J., Rodríguez, E., Shepherd, G. G., Sargoytchev, S., Shepherd, M. G.,
659 Aushev, V. M., Brown, S., García-Comas, M., and Wiens, R. H.: Tidal variations of O₂
660 Atmospheric and OH(6-2) airglow and temperature at mid-latitudes from SATI observations,
661 *Ann. Geophys.*, **23**, 3579–3590, 2005.

662

663 Lopez-Gonzalez, M. J., Rodríguez, E., García-Comas, M., Costa, V., Shepherd, M. G.,
664 Shepherd, G. G., Aushev, V. M., and Sargoytchev, S.: Climatology of planetary wave type
665 oscillations with periods of 2-20 days derived from O₂ atmospheric and OH(6-2) airglow
666 observations at mid-latitude with SATI, *Ann. Geophys.*, **27**, 3645–3662, 2009.

667

668 Lübken, F.-J.: Seasonal variation of turbulent energy dissipation rates at high latitudes as
669 determined by in situ measurements of neutral density fluctuations, *J. Geophys. Res.*, **102**,
670 13,441-13,456, 1997.

671

672 McDade, I. C., Murtagh, D. P., Greer, R. G. H., Dickinson, P. H. G., Witt, G., Stegman, J.,
673 Llewellyn, E. J., Thomas, L., and Jenkins, D. B.: ETON 2: Quenching parameters for the
674 proposed precursors of O₂(b¹Σ_g⁺) and O(¹S) in the terrestrial nightglow, *Planet. Space Sci.*,
675 **34**, 789–800, 1986.

676

677 Mlynczak, M. G., Morgan, F., Yee, J.-H., Espy, P., Murtagh, D., Marshall, B., Schmidlin, F.:
678 Simultaneous measurements of the O₂(¹Δ) and O₂(¹Σ) airglows and ozone in the daytime
679 mesosphere, *Geophys. Res. Lett.*, **28**, 999-1002, 2001.

680

681 Murtagh, D. P., Witt, G., Stegman, J., McDade, I. C., Llewellyn, E. J., Harris, F., and Greer,
682 R. G. H.: An assessment of proposed O(¹S) and O₂(b¹Σ_g⁺) nightglow excitation parameters,
683 *Planet. Space Sci.*, **38**, 1, 45–53, 1990.

684

685 Newnham, D. A. and Balard, J.: Visible absorption cross sections and integrated absorption
686 intensities of molecular oxygen (O₂ and O₄), *J. Geophys. Res.*, **103(D22)**, 28801-28815, 1998.

687

688 Noxon, J. F.: Effect of Internal Gravity Waves Upon Night Airglow Temperatures, *Geophys.*
689 *Res. Lett.*, **5**, 25–27, 1978.

690

691 Ogryzlo, E. A., Shen, Y. Q., and Wassel, P. T.: The yield of $O_2(b^1\Sigma_g^+)$ in oxygen atom
692 recombination, *J. Photochem.*, **25**, 389, 1984.

693

694 Picone, J. M., Hedin, A. E., Drob, D. P., and Aikin, A. C.: NRLMSISE-00 empirical model of
695 the atmosphere: Statistical comparisons and scientific issues, *J. Geophys. Res.*, **107**, 1468,
696 doi:10.1029/2002JA009430, 2002.

697

698 Rapp, M, and Lübken, F.-J.: Polar mesosphere summer echoes (PMSE): Review of
699 observations and current understanding, *Atmos. Chem. Phys.*, **4**, 2601-2633, 2004

700

701 Rodrigo, R., Lopez-Gonzalez, M. J., and Lopez-Moreno, J. J.: Variability of the neutral
702 mesospheric and lower thermospheric composition in the diurnal cycle, *Planet. Space Sci.*,
703 **39**, 803, 1991.

704

705 Sheese, P. E., Llewellyn, E. J., Gattinger, R. L., Bourassa, A. E., Degenstein, D. A., Lloyd, N.
706 D., and McDade I. C.: Temperatures in the upper mesosphere and lower thermosphere from
707 OSIRIS observations of O_2 A-band emission spectra, *Can. J. Phys.*, **88**, 919–925,
708 doi:10.1139/P10-093, 2010.

709

710 Sheese, P. E., Llewellyn, E. J., Gattinger, R. L., Bourassa, A. E., Degenstein, D. A., Lloyd, N.
711 D., and McDade I. C.: Mesopause temperatures during the polar mesospheric cloud season,
712 *Geophys. Res. Lett.*, **38**, L11803, doi:10.1029/2011GL047437. 2011.

713

714 Shepherd, M. G., Cho, Y.-M., Shepherd, G. G., Ward, W., and Drummond, J. R.:
715 Mesospheric temperature and atomic oxygen response during the January 2009 major
716 stratospheric warming, *J. Geophys. Res.*, **115**, A07318, doi:10.1029/2009JA015172, 2010.
717

718 Slanger, T. G. and Black, G.: Interactions of $O_2(b^1\Sigma_g^+)$ with $O(^3P)$ and O_3 . *J. Chem. Phys.*, **70**,
719 3434-3438, 1979.
720

721 Slanger, T. G., Bischel, W. K., and Dyer, M. J.: Photoexcitation of O_2 at 249.3 nm, *Chem.*
722 *Phys. Lett.*, **108**, 472, 1984.
723

724 Smith, A. K., Marsh, D. R., Mlynczak, M. G., and Mast J. C.: Temporal variation of atomic
725 oxygen in the upper mesosphere from SABER, *J. Geophys. Res.*, **115**, D18309,
726 doi:10.1029/2009JD013434, 2010.
727

728 Smith, I. W. M.: The role of electronically excited states in recombination reactions, *Int. J.*
729 *Chem. Phys.*, **16**, 423–443, 1984.
730

731 Strelnikov, B., Rapp, M., and Lübken, F.-J.: In-situ density measurements in the
732 mesosphere/lower thermosphere region with the TOTAL and CONE instruments, in: An
733 Introduction to Space Instrumentation, edited by: Oyama, K., Terra Publishers,
734 doi:10.5047/isi.2012.001, 2013. <http://www.terrapub.co.jp/onlineproceedings/st/aisi/>
735

736 Strelnikov, B., Szewczyk, A., Strelnikova, I., Latteck, R., Baumgarten, G., Lübken, F.-J.,
737 Rapp, M., Fasoulas, S., Löhle, S., Eberhart, M., Hoppe, U.-P., Dunker, T., Friedrich, M.,
738 Hedin, J., Khaplanov, M., Gumbel, J., and Barjatya, A.: Spatial and temporal variability in
739 MLT turbulence inferred from in situ and ground based observations during the WADIS-1

740 sounding rocket campaign, *Ann. Geophys.*, **35**, 547–565, doi:10.5194/angeo-35-547-2017,
741 2017.

742

743 Strelnikov, B., Staszak, T., Strelnikova, I., Lübken, F.-J., Grygalashvyly, M., Hedin, J.,
744 Khaplanov, M., Gumbel, J., Fasoulas, S., Löhle, S., Eberhart, M., Baumgarten, G., Höffner,
745 J., Wörl, R., Rapp, M., and Friedrich, M.: Simultaneous in situ measurements of small-scale
746 structures in neutral, plasma, and atomic oxygen densities during WADIS sounding rocket
747 project, *Atmos. Chem. Phys.*, submitted , 2018.

748

749 Tarasick, D. W. and Shepherd, G. G.: Effects of gravity waves on complex airglow
750 chemistries. 2. OH emission, *J. Geophys. Res.*, **97**, 3195-3208, 1992.

751

752 Viereck, R. A. and Deehr, C. S.: On the interaction between gravity waves and the OH Meinel
753 (6-2) and O₂ Atmospheric (0-1) bands in the polar night airglow, *J. Geophys. Res.*, **94**, 5397–
754 5404, 1989.

755

756 Vorobeva, E., Yankovsky, V., and Schayer, V.: Estimation of uncertainties of the results of
757 [O(³P)], [O₃] and [CO₂] retrievals in the mesosphere according to the YM2011 model by two
758 approaches: sensitivity study and Monte Carlo method, EGU General Assembly, Vienna,
759 Austria, 8–13 April 2018, EGU2018-AS1.31/ST3.7-17950,
760 https://presentations.copernicus.org/EGU2018-17950_presentation.pdf, 2018.

761

762 Wildt, J., Bednarek, G., Fink, E. H., Wayne, R. P.: Laser excitation of the A³Σ_u⁺, A¹Δ_u and
763 c¹Σ_u⁻ states of molecular oxygen, *Chem. Phys.*, **156(3)**, 497-508, doi: 10.1016/0301-
764 0104(91)89017-5, 1991.

765

766 Witt, G., Stegman, J., Murtagh, D. P., McDade, I. C., Greer, R. G. H., Dickinson, P. H. G.,
767 and Jenkins, D. B.: Collisional energy transfer and the excitation of $O_2(b^1\Sigma_g^+)$ in the
768 atmosphere, *J. Photochem.*, **25**, 365, 1984.

769
770 Wraight, P. C.: Association of atomic oxygen and airglow excitation mechanisms, *Planet.*
771 *Space Sci.*, **30(3)**, 251-259, 1982.

772
773 Yankovsky, V. A. and Manuilova, R. O.: Possibility of simultaneous $[O_3]$ and $[CO_2]$ altitude
774 distribution retrievals from the daytime emissions of electronically-vibrationally excited
775 molecular oxygen in the mesosphere, *J. Atmos. Sol.-Terr. Phys.*, **179**, 22-33, doi:
776 10.1016/j.jastp.2018.06.008, 2018.

777
778 Yankovsky, V. A., Martysenko, K. V., Manuilova, R. O., and Feofilov, A. G.: Oxygen
779 dayglow emissions as proxies for atomic oxygen and ozone in the mesosphere and lower
780 thermosphere, *J. Mol. Spectrosc.*, **327**, 209–231, doi:10.1016/j.jms.2016.03.006, 2016.

781
782 Young, R. A. and Sharpless, R. L.: Chemiluminescence and reactions involving atomic
783 oxygen and nitrogen, *J. Chem. Phys.*, **39**, 1071, 1963.

784
785 Young, R. A. and Black, G.: Excited state formation and destruction in mixtures of atomic
786 oxygen and nitrogen, *J. Chem. Phys.*, **44**, 3741, 1966.

787
788 Zagidullin, M. V., Khvatov, N. A., Medvedkov, I. A., Tolstov, G. I., Mebel, A. M., Heaven,
789 M. C., and Azyazov, V. N.: $O_2(b^1\Sigma_g^+)$ Quenching by O_2 , CO_2 , H_2O , and N_2 at Temperatures
790 of 300–800 K, *J. Phys. Chem.*, **121 (39)**, 7343-7348, doi: 10.1021/acs.jpca.7b07885, 2017.

791

792 Zarboo, A., Bender, S., Burrows, J. P., Orphal, J., and Sinnhuber, M.: Retrieval of O₂(¹Σ) and
793 O₂(¹Δ) volume emission rates in the mesosphere and lower thermosphere using
794 SCIAMACHY MLT limb scans, *Atmos. Meas. Tech.*, **11**, 473-487,
795 <https://doi.org/10.5194/amt-11-473-2018>, 2018.

796

797 Zhang, S. P., Wiens, R. H., and Shepherd, G. G.: Gravity waves from O₂ nightglow during the
798 AIDA '89 campaign II: numerical modeling of the emission rate/temperature ratio, η , *J.*
799 *Atmos. Terr. Phys.*, **55**, 377–395, 1993.

800

801

802

803

804

805

806

807

808

809

810

811

812

813

814

815

816 **Table 1.** List of reactions with corresponding reaction rates (for three-body reactions [cm^6
817 $\text{molecule}^{-2} \text{s}^{-1}$] and for two-body reactions [$\text{cm}^3 \text{molecule}^{-1} \text{s}^{-1}$]), quenching coefficients, and
818 spontaneous emission coefficients (s^{-1}) used in the paper.

	Reaction	Coefficient	Reference
R1	$O + O + M \xrightarrow{\varepsilon k_1} O_2(b^1\Sigma_g^+) + M$	$k_1 = 4.7 \cdot 10^{-33} (300/T)^2$ $\varepsilon - \text{unknown}$	Campbel and Gray (1973)
R2	$O_2(b^1\Sigma_g^+) + O_2 \xrightarrow{k_2^{O_2}} \text{products}$	$k_2^{O_2}$ $= 7.4 \cdot 10^{-17} T^{0.5} e^{-\frac{1104.7}{T}}$	Zagidullin et al. (2017)
R3	$O_2(b^1\Sigma_g^+) + N_2 \xrightarrow{k_2^{N_2}} \text{products}$	$k_2^{N_2} = 8 \cdot 10^{-20} T^{1.5} e^{\frac{503}{T}}$	Zagidullin et al. (2017)
R4	$O_2(b^1\Sigma_g^+) + O \xrightarrow{k_2^O} \text{products}$	$k_2^O = 8 \cdot 10^{-14}$	Slanger and Black (1979)
R5	$O_2(b^1\Sigma_g^+) \xrightarrow{A_1} O_2 + h\nu(762\text{nm})$	$A_1 = 0.0834$	Newnham and Ballard (1998)
R6	$O_2(b^1\Sigma_g^+) \xrightarrow{A_2} O_2 + h\nu(\text{total})$	$A_2 = 0.088158$	Yankovsky et al. (2016)
R7	$O + O + M \xrightarrow{\alpha k_1} O_2^* + M$	$\alpha - \text{unknown}$	
R8	$O_2^* + O_2 \xrightarrow{\gamma k_3^{O_2}} O_2(b^1\Sigma_g^+) + O_2$	$\gamma - \text{unknown}$	
R9	$O_2^* + O_2, N_2, O \xrightarrow{k_3^{O_2}, k_3^{N_2}, k_3^O} \text{prod.}$	$k_3^{O_2}, k_3^{N_2}, k_3^O - \text{unknown}$	
R10	$O_2^* \xrightarrow{A_3} O_2 + h\nu$	$A_3 - \text{unknown}$	

819

820 **Table 2.** Efficiencies α of the different excited states of O_2 .

$O_2(c^1\Sigma_u^-)$	$O_2(A'^3\Delta_u)$	$O_2(A^3\Sigma_u^+)$	$O_2(^5\Pi_g)$	Reference
0.03	0.12	0.04	0.66	Wraight (1982), Smith (1984)
0.04	0.18	0.06	0.5	Bates (1988)
0.03	0.18	0.06	0.52	López-González et al. (1992a, b, c)

821

822 **Table 3.** Fitting coefficients for combined mechanism (Eq. 5) at different efficiencies.

	Low $\tilde{\varepsilon}$ Wraight (1982)	High $\tilde{\varepsilon}$ Bates (1988)	Averaged $\tilde{\varepsilon}$ (this work)
$\tilde{\varepsilon}$	0.015	0.03	0.022
$D_1 = \tilde{k}_3^O / \tilde{k}_3^{O_2}$	$0.211^{+0.355}_{-0.136}$	$0.397^{+0.22}_{-0.282}$	$0.231^{+0.358}_{-0.142}$
$D_2 = \tilde{\alpha}\tilde{\gamma}$	$0.087^{+0.12}_{-0.041}$	$0.073^{+0.119}_{-0.042}$	$0.08^{+0.12}_{-0.04}$

823

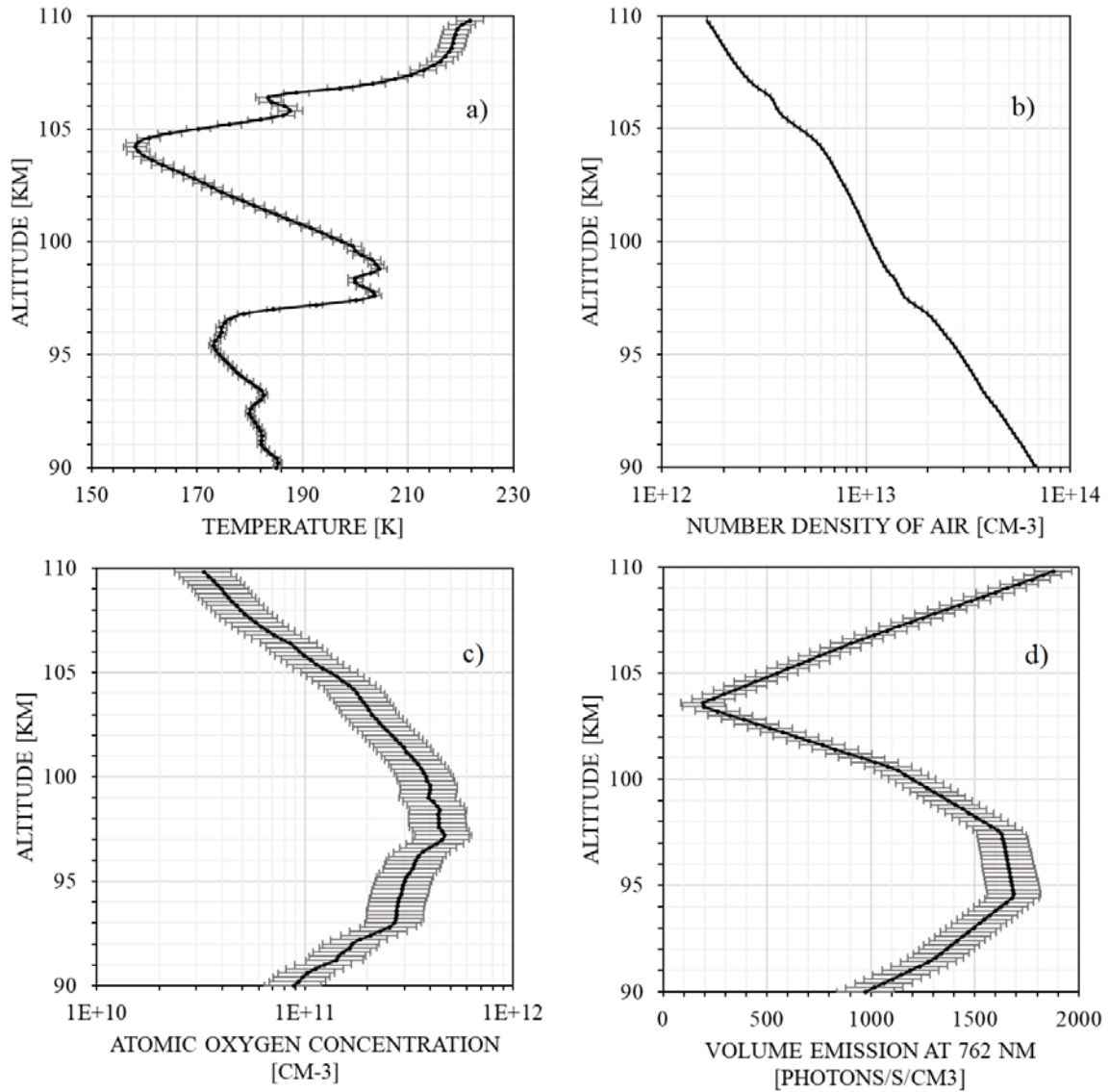
824

825

826 **Figures.**

827 Figure 1. Measurements of a) temperature (CONE), b) number density of air (CONE), c)

828 atomic oxygen concentration (FIPEX), d) volume emission at 762 nm (photometer).



829

830

831

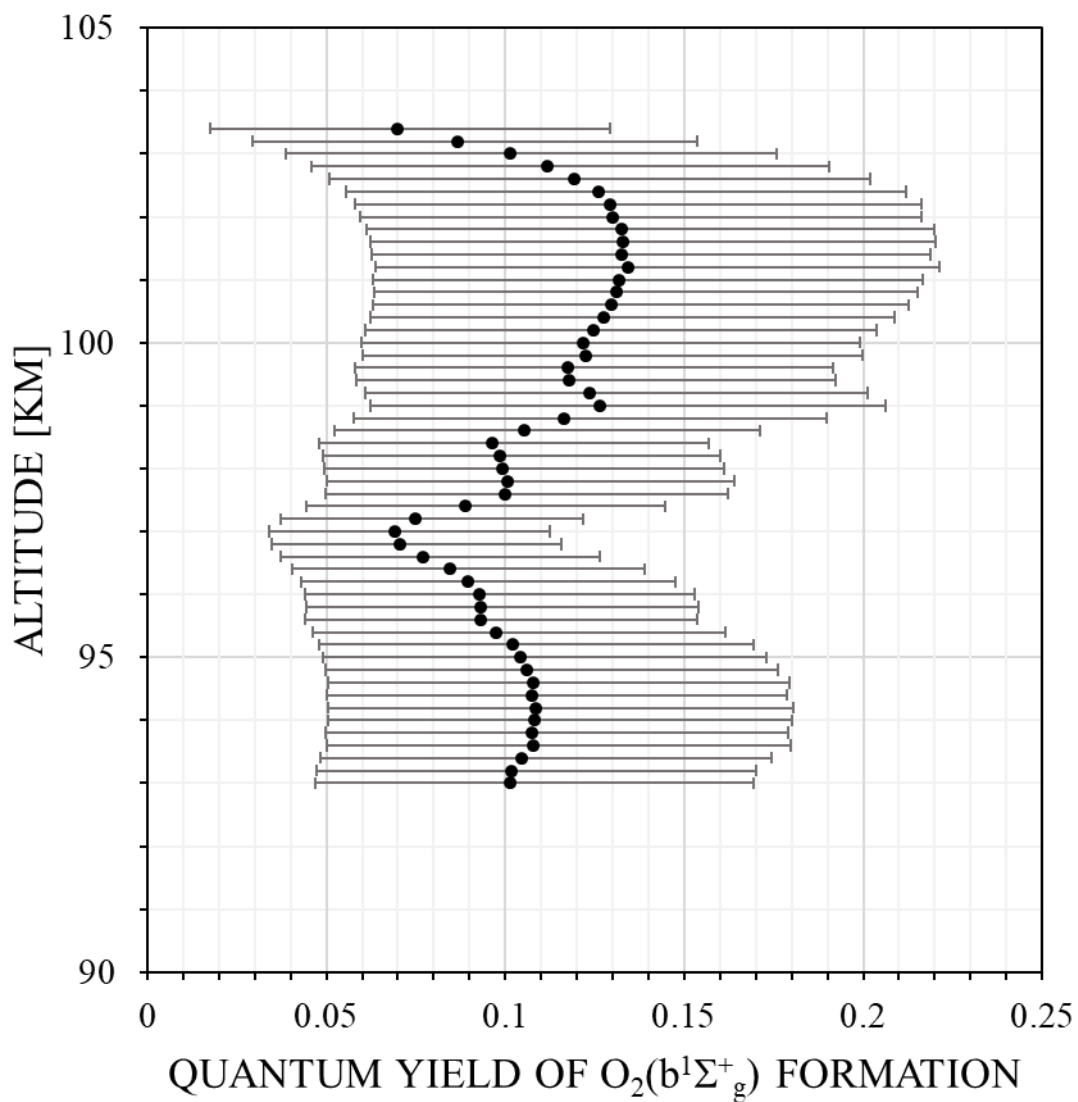
832

833

834

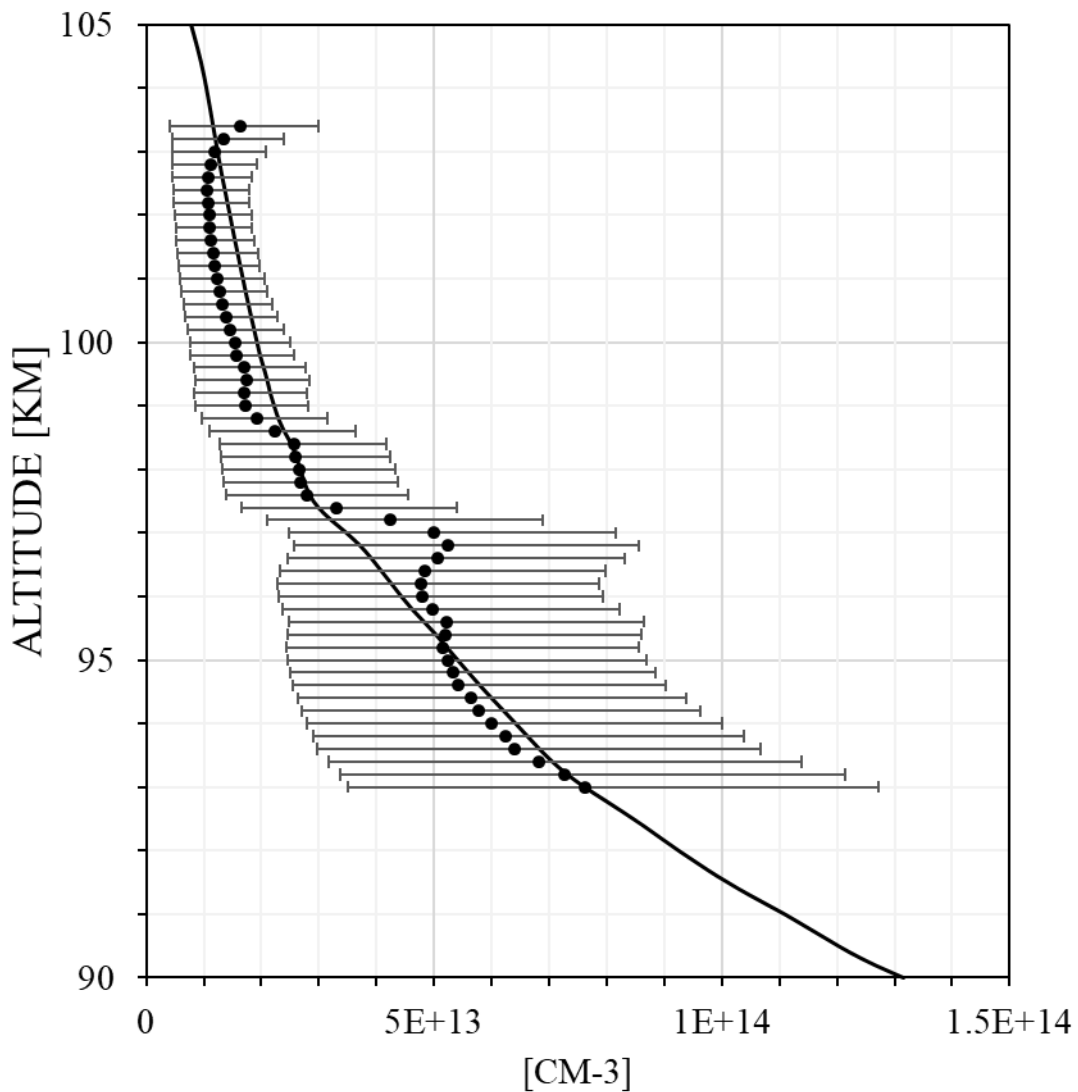
835

836 Figure 2. Quantum yield of $O_2(b^1\Sigma_g^+)$ formation ε for the case of one-step mechanism.



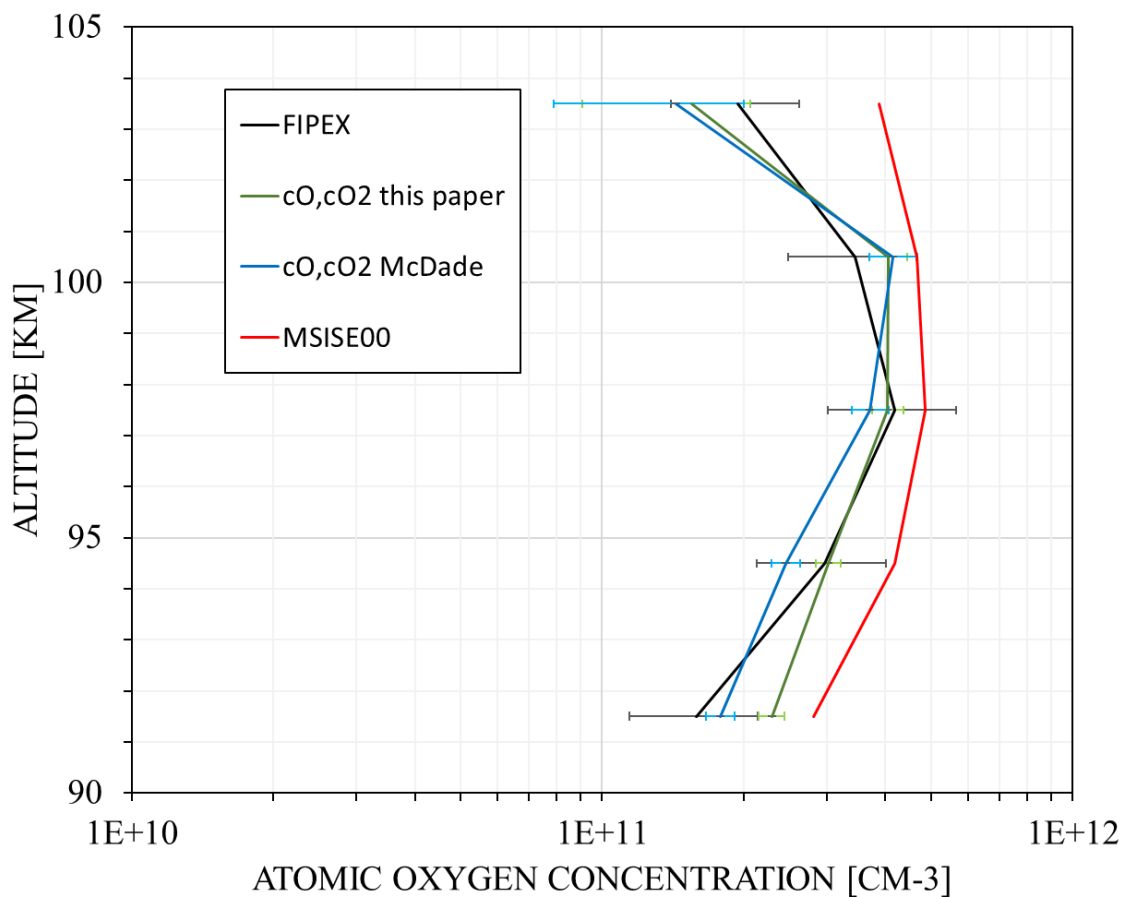
837
838
839
840
841
842
843
844
845
846

847 Figure 3. RHS (dots) and least-square fit of LHS (black line) of equation (4).



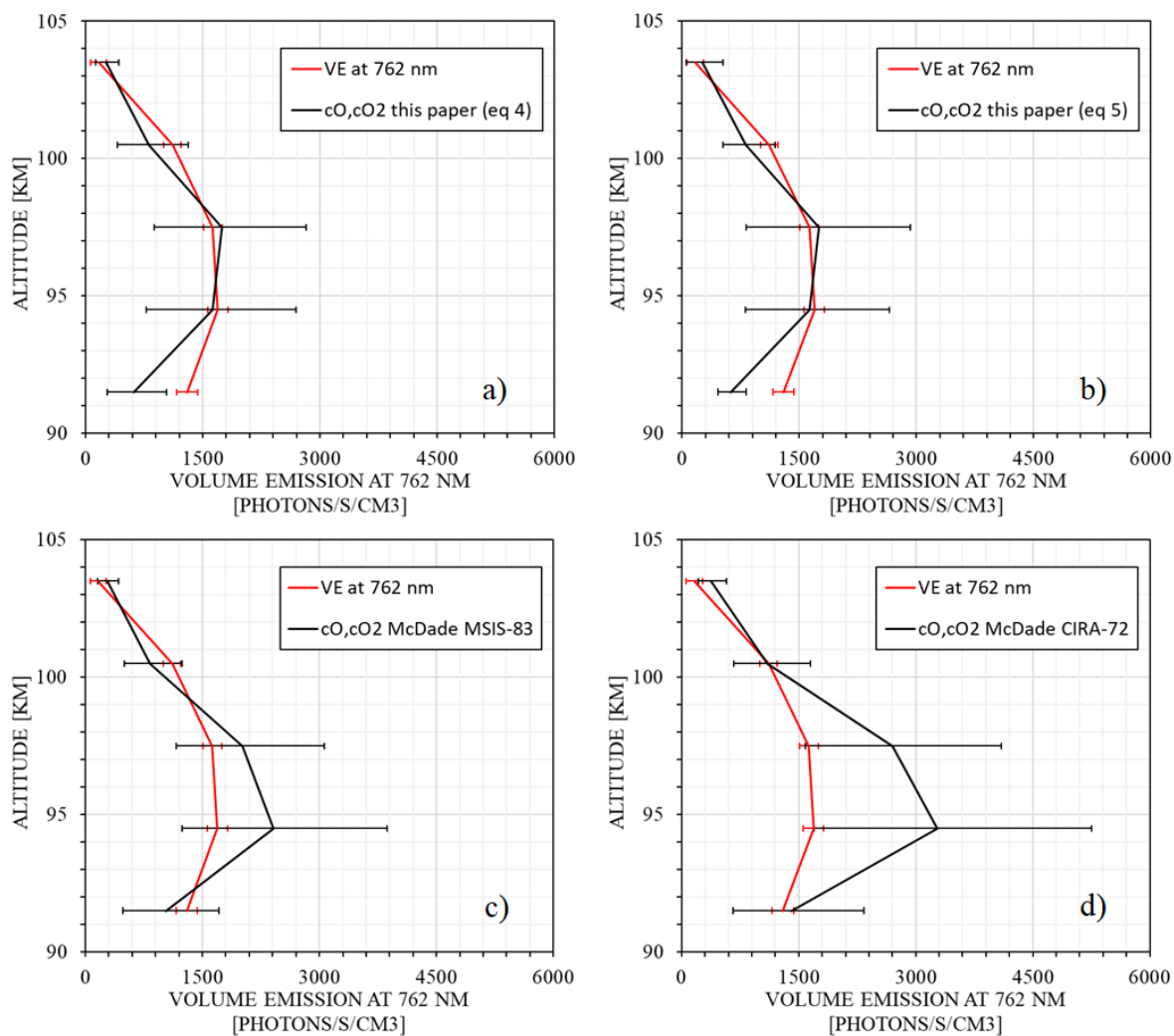
848
849
850
851
852
853
854
855
856
857

858 Figure 4. Atomic oxygen concentration: FIPEX (black line); model MSISE00 (red line);
859 derived from emission observation with McDade et al. (1986) coefficients (blue line);
860 calculated with newly derived fitting coefficients for the two-step mechanism (green line).



861
862
863
864
865
866
867
868
869
870
871

872 Figure 5. Volume emissions: photometer (red line); derived from atomic oxygen (black line)
 873 with a) newly derived fitting coefficients for the two-step mechanism, b) with fitting
 874 coefficients for combined mechanism, c) with McDade et al. (1986) coefficients, which
 875 correspond to the MSIS-83 temperature, and with McDade et al. (1986) coefficients, which
 876 correspond to the CIRA-72 temperatures.



877